Available online at www.sciencedirect.com
ScienceDirect
Journal of Power Sources 164 (2007) 561–566
JOURNAL OF POWER SOURCES
www.elsevier.com/locate/jpowsour

Short communication

Electron transport in direct methanol fuel cells

Wenpeng Liu [a,*], Chao-Yang Wang [b]

[a] *MTI Micro Fuel Cells Inc., 431 New Karner Road, Albany, NY 12205, USA*
[b] *Electrochemical Engine Center (ECEC), and Department of Mechanical and Nuclear Engineering, The Pennsylvania State University, University Park, PA 16802, USA*

Received 25 September 2006; received in revised form 19 November 2006; accepted 20 November 2006
Available online 29 December 2006

Abstract

A three-dimensional (3D), two-phase, isothermal model of direct methanol fuel cells (DMFCs) was employed to investigate effects of electron transport through the backing layer and the land in bipolar plates. It was found that the electronic resistance of the backing layer, affected by backing layer electronic conductivity, backing layer thickness and flow channel width, played a relatively important role in determining the current density distribution and cell performance. In order to ignore the electron transport effect on the average current density, the minimum electronic conductivity of the backing layer has to be 1000 S m^{-1}, with the relative error in the average current density less than 5%, under the given conditions.

Keywords: Direct methanol fuel cell; Electron transport; Modeling; Three dimensions

1. Introduction

As a promising candidate for next-generation portable power sources, the direct methanol fuel cell (DMFC) has attracted tremendous research and industrial interests. However, in order to compete with lithium-ion batteries, a portable DMFC system must overcome several key technical challenges, i.e., low rate of methanol oxidation kinetics, methanol and water crossover, thermal management, and catalyst poisoning and loading issues. As a result, there is an urgent need for understanding, prediction, and optimization of various interactive transport and electrochemical processes that occur in portable DMFCs.

Focusing on either one or two dimensions, early DMFC models [1–6] were developed to study the mass transport phenomena, electrochemical processes, and their interactions, without considering two-phase effects, which is found to be of paramount importance to understand DMFC behaviors. Meyers and Newman [7–9] developed a theoretical framework that describes the equilibrium of multicomponent species in the membrane in a three-part series. However, the effect of flow and stoichiometry was not considered.

In recently developed 3D polymer electrolyte fuel cell (PEFC) models, computational fluid dynamics (CFD) methodology has been employed to integrate electrochemical processes with water/proton co-transport to enable multiphysics modeling and large-scale simulation. However, compared with H_2/air PEFCs, the 3D mathematical modeling has not been widely applied to DMFCs, due to more complex interactions between two-phase species transport and electrochemical reactions. Most recently, Liu and Wang [10] presented a 3D, two-phase DMFC model, based on multi-phase mixture (M^2) modeling framework of Wang et al. [11–13], to reveal an intricate interaction between species transport and electrical current in three dimensions. This model has been extended to further study the net water transport coefficient distribution and interfacial liquid water coverage effect by Liu and Wang [14]. A more complete review of DMFC modeling in the literature is recently given by Wang [15].

Among the 3D DMFC models published to date, electron transport in the catalyst and backing layers, and in the bipolar plate is ignored by assuming a sufficiently large electronic conductivity and consequently constant electronic phase potential in these materials. This assumption is valid likely in the lands in the through-plane direction, of which the electronic conductivity is of the order of 20,000 S m^{-1} for graphite plates, but could be inappropriate in the backing and catalyst layers, in which the effective electronic conductivities range only from 300 to

* Corresponding author. Tel.: +1 518 533 2232; fax: +1 518 533 2223.
E-mail address: wliu@mechtech.com (W. Liu).

0378-7753/$ – see front matter © 2006 Elsevier B.V. All rights reserved.
doi:10.1016/j.jpowsour.2006.11.032

Nomenclature

aj_0	total exchange current density (A m^{-3})
c	molar concentration (mol m^{-3})
D	diffusivity (m^2 s^{-1})
F	Faraday's constant (96485 C mol^{-1})
i	operating current density (A m^{-2})
j	volumetric current density (A m^{-3})
K_c	reaction constant
$\dot{m}$	mass source term in governing equations
n_d	electro-osmotic drag coefficient
p	pressure (Pa)
R_i	ohmic resistance (i = *land, backing or channel*) (Ω m^2)
s	liquid water saturation
S^k	molar source term of k species
$\mathbf{u}$	velocity (m s^{-1})
U^0	standard equilibrium potential (V)
V_{cell}	cell voltage (V)
Z	width (in-plane direction) (m)

Greek letters

α_i	current transfer coefficient at anode or cathode ($i = a$ or c)
δ	thickness (m)
ε	porosity of porous medium
Φ	phase potential (V)
γ	advection correction factor
η_i	overpotential of anode or cathode ($i = a$ or c) (V)
κ	ionic conductivity of membrane (S m^{-1})
ρ	density (kg m^{-3})
σ	electronic conductivity of electrode (S m^{-1})

Subscripts

a	anode
c	cathode
cata	catalyst layer
e	electrolyte
eff	effective
g	gas phase
int	interface
l	liquid phase
m	membrane
s	solid or electronic phase
xover	crossover

Superscripts

MeOH	methanol
O_2	oxygen
k	species
ref	reference

500 S m^{-1} in the through-plane direction. In recent studies of modeling on PEFCs, the electron transport in PEFCs has been addressed [16–21]. It was concluded that by solving the electron transport equation in the catalyst layers, the gas diffusion layers (GDL), and the current collecting plates on both anode and cathode sides, it enabled further capabilities in modeling fuel cells, including direct incorporation of the contact resistances between the membrane electrode assembly (MEA) and GDL, and between GDL and the current collecting land.

In this paper, a 3D isothermal, electrochemical and transport fully coupled DMFC model is described, with focus on electron transport. Additional to the complete set of conservation equations of mass, momentum, and species presented in [10], an electron transport equation is included in the catalyst and backing layers, and the land in bipolar plates in order to investigate the effects of electronic resistance in the DMFC. At the same time, a proton transport equation is solved inside MEA to accurately account for electrolyte ionic resistance. The effects of the lateral electronic resistance on the current distribution and cell performance are studied in detail.

2. Model development

The two-phase steady-state DMFC model in this work consists of nonlinear, coupled partial differential equations of conservation of mass, momentum and species. These can be presented in concise form as follows [10]:

$$\text{Continuity}: \quad \frac{\partial(\varepsilon\rho)}{\partial t} + \nabla\cdot(\rho\mathbf{u}) = \dot{m} \tag{1}$$

$$\text{Momentum}: \quad \frac{1}{\varepsilon}\left[\frac{\partial(\rho\mathbf{u})}{\partial t} + \frac{1}{\varepsilon}\nabla\cdot(\rho\mathbf{u}\mathbf{u}) = -\nabla p + \nabla\cdot\tau + S_u\right] \tag{2}$$

$$\text{Species}: \quad \frac{\partial c^k}{\partial t} + \nabla\cdot\{\gamma\mathbf{u}c^k\} = \nabla\cdot[D^k_{l,\text{eff}}\nabla c^k_l + D^k_{g,\text{eff}}\nabla c^k_g] - \nabla\cdot\left[\left(\frac{c^k_l}{\rho_l} - \frac{c^k_g}{\rho_g}\right)\boldsymbol{j}_l\right] + S^k \tag{3}$$

where ρ, $\mathbf{u}$, and c^k denote the two-phase mixture density, velocity vector and molar concentration of species k, respectively. The species considered here are methanol, water, and oxygen. The various two-phase properties, source terms, and thermophysical properties identified for various regions of a DMFC, as well as necessary boundary conditions, have been detailed in [10–13] and thus are not repeated here:

$$\text{Proton transport}: \quad 0 = \nabla\cdot(\kappa_{\text{eff}}\nabla\Phi_e) + S_\Phi \tag{4}$$

$$\text{where} S_\Phi = \begin{cases} j & \text{anode catalyst layer} \\ -j_c + j_{\text{xover}} & \text{cathode catalyst layer} \end{cases}$$

This equation indicates that protons are generated in the anode catalyst layer and consumed in the cathode catalyst layer. In the cathode catalyst layer source term, the methanol crossover flux through the membrane, j_{xover}, is caused by electro-osmotic drag and diffusion, given by

$$\frac{j_{\text{xover}}}{6F} = \nabla\left(n_d^{\text{MeOH}}\frac{i}{F}\right) + \frac{D_m^{\text{MeOH}}(c_l^{\text{MeOH}}|_{\text{int}}/\delta_m)}{\delta_{\text{cata}}} \tag{5}$$

In additional to proton transport, an electron transport equation is employed in the current 3D model, which will be solved numerically in the backing and catalyst layers, as well as in current collecting lands on both anode and cathode sides in order to fully investigate its effect on the current distribution and cell performance:

$$\text{Electron transport}: \quad 0 = \nabla \cdot (\sigma_{s,\text{eff}} \nabla \Phi_s) + S_\Phi \tag{6}$$

where

$$S_\Phi = \begin{cases} -j & \text{anode catalyst layer} \\ j_c - j_{\text{xover}} & \text{cathode catalyst layer} \end{cases}$$

The source terms in the above equation correspond to the methanol oxidation and oxygen reduction reactions, creating or consuming electrons in either anode or cathode catalyst layer. Note also that electrons always flow from low potential to high potential location.

Electrochemical kinetics in the proton and electron equations is expressed by Tafel approximations of Butler–Volmer equation in the anode and cathode, respectively, such that

$$j = \frac{a j_{o,a}^{\text{ref}} c_1^{\text{MeOH}}|_{\text{cata}} \exp((\alpha_a F/RT)\eta_a)}{c_1^{\text{MeOH}}|_{\text{cata}} + K_c \exp((\alpha_a F/RT)\eta_a)} \tag{7}$$

where $\eta_a = \Phi_s - \Phi_e - U_a^0$ with $\Phi_s = 0$ at anode current collecting land boundary.

And

$$j_c = j + j_{\text{xover}} = a j_{o,c}^{\text{ref}} \left(\frac{c_g^{O_2}|_{\text{cata}}}{c_g^{O_2,\text{ref}}} \right) (1-s) \exp\left(-\frac{\alpha_c F}{RT} \eta_c \right) \tag{8}$$

where $\eta_c = \Phi_s - \Phi_e - U_c^0$ with $\Phi_s = V_{\text{cell}}$ at cathode current collecting land boundary.

As can be seen, besides intricate couplings between species transport equations, a numerical problem unique to 3D modeling of DMFC is the strong coupling between the species transport equations and electrochemical kinetics that are dependent on species concentrations. Therefore, the model must seek a stable and efficient solution procedure.

In this paper, the present DMFC model is implemented into commercial software, Fluent, through user-defined functions, or UDFs, provided by Fluent in DEFINE macros, which are employed to implement sources terms, diffusion coefficients, material properties, and boundary conditions. The species equations of methanol, water and oxygen, as well as the proton and electron transport equations, are implemented using user-defined scalars (UDS). More detailed numerical procedures have been described in [10].

3. Results and discussion

3.1. Theoretical analysis

Fig. 1 displays a schematic of the current collecting land and backing layer. The typical thickness of the land (δ_{land}) is 2 mm,

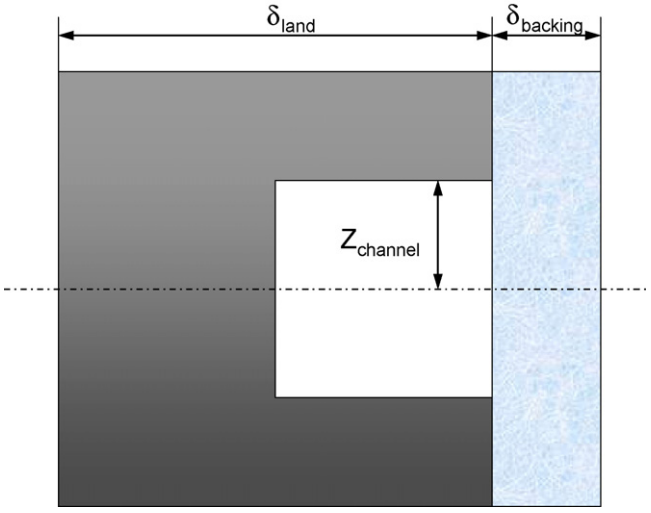

Fig. 1. Schematic of the current collecting land and backing layer.

thickness of the backing layer (δ_{backing}) is 0.3 mm and the half-width of the flow channel (Z_{channel}) is 0.5 mm. If the effective electronic conductivities of the land in the bipolar plate (i.e. graphite) and backing layer (i.e. carbon paper) are assumed to be 20,000 and 300 S m^{-1}, respectively, the typical electronic resistance in the current collecting land, R_{land}, can thus be calculated as

$$R_{\text{land}} = \frac{\delta_{\text{land}}}{\sigma_{\text{land}}} = \frac{2\,\text{mm}}{20000\,\text{S m}^{-1}} = 1\,\text{m}\Omega\,\text{cm}^2 \tag{9}$$

This indicates that the electron resistance in the land is very small, and therefore, always negligible.

The ohmic resistance across the backing layer in the through-plane direction, R_{backing}, is

$$R_{\text{backing}} = \frac{\delta_{\text{backing}}}{\sigma_{\text{backing}}} = \frac{0.3\,\text{mm}}{300\,\text{S m}^{-1}} = 10\,\text{m}\Omega\,\text{cm}^2 \tag{10}$$

And, the electronic resistance of the backing layer in the in-plane direction, R_{channel}, is

$$R_{\text{channel}} = \frac{Z_{\text{channel}}}{\sigma_{\text{backing}}} = \frac{0.5\,\text{mm}}{300\,\text{S m}^{-1}} = 16.7\,\text{m}\Omega\,\text{cm}^2 \tag{11}$$

The electron phase potential variation is proportional to both electron resistance and average current density. Since the average current densities in the through-plane and in-plane directions are different, the electronic resistances along the two directions, R_{backing} and R_{channel}, are not directly comparable. Assuming that the average current density under the gas channel is a constant $\bar{i}$, and the average current density through the backing layer thickness is uniform, the lateral electronic phase potential variation in the backing layer can then be derived as

$$\Delta\Phi_s = \int_0^{Z_{\text{channel}}} \frac{\bar{i} z}{\delta_{\text{backing}} \sigma_{\text{backing}}} \,\text{d}z = \bar{i} R_{\text{channel}} \frac{Z_{\text{channel}}}{2\delta_{\text{backing}}} \tag{12}$$

A scaling factor should, therefore, be included in the lateral electronic resistance. The modified lateral electronic resistance

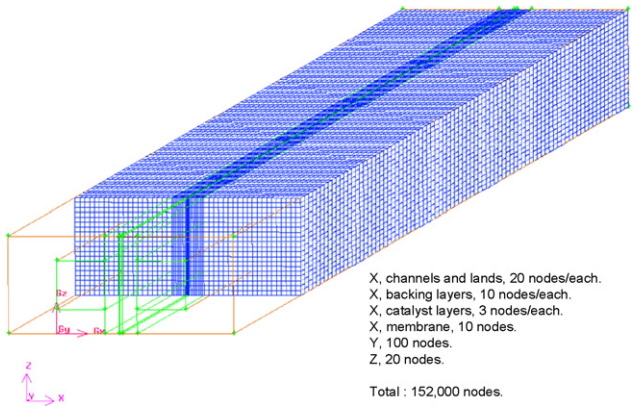

Fig. 2. Numerical mesh used for 3D simulations.

is

$$R'_{\text{channel}} = R_{\text{channel}} \frac{Z_{\text{channel}}}{2\delta_{\text{backing}}} = 16.7 \frac{0.5\,\text{mm}}{2\,\text{mm} \times 0.3\,\text{mm}} = 13.9\,\text{m}\Omega\,\text{cm}^2 \quad (13)$$

From Eqs. (10) and (13), it is clear that both through-plane and in-plane electronic resistances are sufficiently large enough to affect the current distribution, not only globally on the cell performance but also locally between a channel and a land in the flow direction.

The parameter of $Z_{\text{channel}}/2\delta_{\text{backing}}$ in Eq. (13), the ratio of the half width of the flow channel to the doubled backing layer thickness, is thus an important variable in the portable DMFC design. At a given flow channel width, the in-plane ohmic drop will increase when decreasing the backing layer thickness. Numerical results presented in the next section reveal that the backing layer functions not only to distribute reactants to catalyst layer but also to provide a path for lateral electron conduction. Note also that the contact resistance causes a resistance increase in the through-plane direction and has a minimal effect on the in-plane direction. However, the effect of the contact resistance is ignored in this study, due to relatively low current density in the DMFC.

3.2. Numerical results and discussions

In order to solve the model in Fluent, a numerical mesh with a total of 152,000 grid points for the 3D single channel DMFC domain is generated in Gambit software, as shown in Fig. 2. This mesh has been tested to be sufficient by a careful grid-independence study. As convergence criteria, we set the residuals for all governing equations less than 10^{-6}. In addition, selected physical properties and electrochemical parameters most relevant to the present simulation results are listed in Tables 1 and 2, respectively.

As shown in Eq. (13), the in-plane electronic resistance is determined by the electronic conductivity, backing layer thickness and flow channel width. A parametric study is conducted to reveal its effect on current density distribution and cell performance. The variation of the in-plane electronic resistance is carried out through changing the backing layer conductivity. The effect should be the same through changing the backing layer thickness and/or the flow channel width, while the latter must involve generation of new numerical meshes, which is rather time consuming. Current density distributions in the middle of the membrane under three different electronic conductivities of the backing layer are shown in Fig. 3. For the electronic conductivity of 300 S m^{-1}, the maximum current density is located under the edges between the gas channel and the current collecting land, as this location offers the best combination of easy access by methanol and a short path for electron transport onto the land. It is clearly shown that in-plane electron transport in the backing layer plays a critical role in determining the current density profile between the channel and the land.

As the electronic conductivity increases to 1000 S m^{-1}, the land effect is weaker, while the methanol transport phenomenon in the in-plane direction becomes more dominant. By assuming an infinitely large electronic conductivity, i.e., completely neglecting electron transport, methanol transport becomes the sole factor determining the current density distribution; as a result, the maximum current density always occurs in the middle of the gas channel. The numerical results further indicate that the widths of the flow channel and current collecting land are key optimization parameters for better cell performance.

Current density profiles along the in-plane direction in the mid-length of the cell under different electronic conductivities

Table 1
Three-dimensional cell geometry and operating conditions

Cell length	0.1 m
Cell width	2×10^{-3} m
Anode channel width	1×10^{-3} m
Anode backing thickness	300×10^{-6} m
Anode catalyst thickness	10×10^{-6} m
Membrane thickness	50×10^{-6} m
Cathode catalyst thickness	10×10^{-6} m
Cathode backing thickness	300×10^{-6} m
Cathode channel width	1×10^{-3} m
Operating temperature	60 °C
Anode channel pressure	1 atm
Cathode channel pressure	1 atm
Flow stoichiometry of anode channel	2
Flow stoichiometry of cathode channel	3
Inlet methanol concentration at anode	2000 mol m^{-3} (2 M)
Inlet liquid saturation at anode	100%
Inlet liquid saturation at cathode	0% (fully humidified air)
Interfacial liquid saturation at the cathode backing layer	0%
Cell operating voltage	0.4 V

Table 2
Electrochemical parameters

Faraday constant	96,485 C mol^{-1}
Gas constant	8.314 J (mol K)$^{-1}$
Anodic transfer coefficient	0.239
Cathodic transfer coefficient	0.875
Proton conductivity of membrane	0.1×10^2 S m^{-1}
Electronic conductivity in current collecting land	20,000 S m^{-1}
Electronic conductivity in GDL	300–∞ S m^{-1}

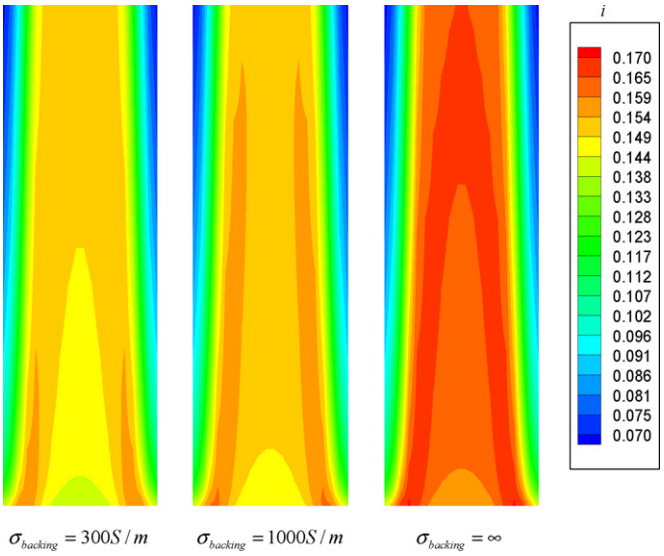

Fig. 3. Current density distribution (A cm^{-2}) in the middle of membrane under different electronic conductivities in the backing layer (at 0.4 V).

of the backing layer are shown in Fig. 4. In order to neglect the electron transport effect, the electronic conductivity of the backing layer has to reach at least 1000 S m^{-1}, at which the relative error in the average current density is less than 5% as compared to the case with an infinitely large electronic conductivity. The average current densities at cell voltage of 0.4 V with different electronic conductivities are listed and compared in Table 3.

The electronic resistance in the backing layer will not only affect the current distribution in the width direction, but also that in the flow direction. The current density distributions in the middle of the membrane under different electronic conductivities in the backing layer in the flow direction are presented in Fig. 5. The current density distributions are all showing a fast increase near the inlet due to the strong methanol crossover, and then

Table 3
Average current densities at cell voltage of 0.4 V with various electronic conductivities of backing layer

Electronic conductivity (S m^{-1})	Average current density (A cm^{-2})	Relative error (%)
∞	0.142	–
1500	0.137	3.5
1000	0.135	4.9
500	0.133	6.3
300	0.132	7.0

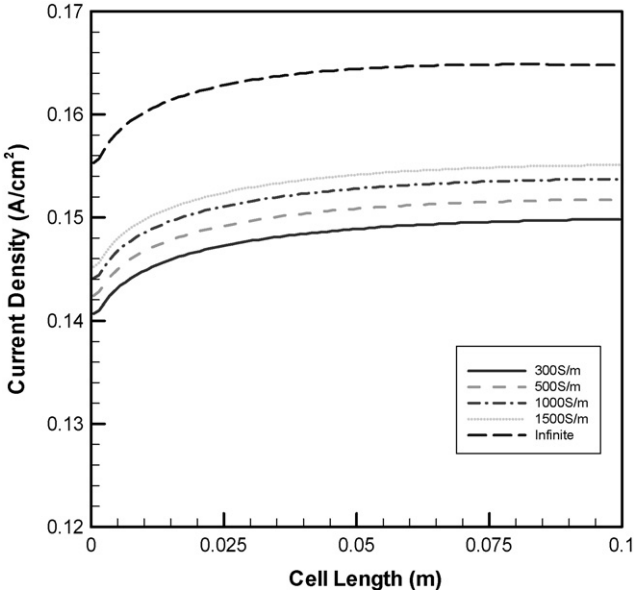

Fig. 5. Current density distributions in middle of cell width along the flow direction for different electronic conductivities in the backing layer.

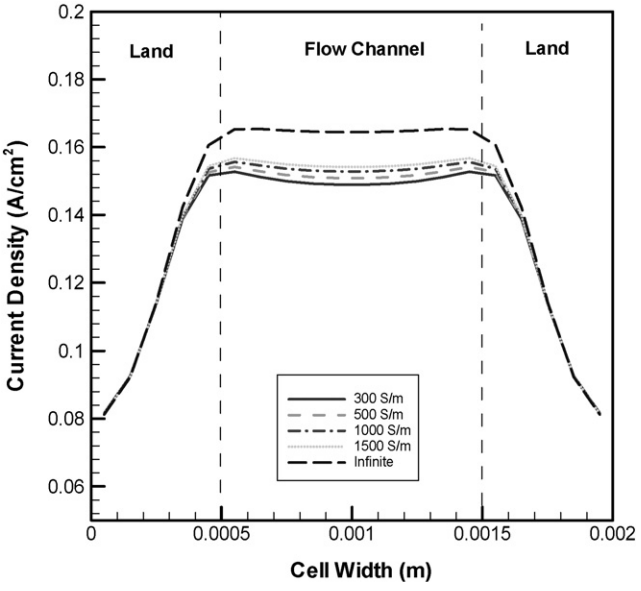

Fig. 4. Current density distribution in the width direction in the mid-length of the cell for different electronic conductivities in the backing layer.

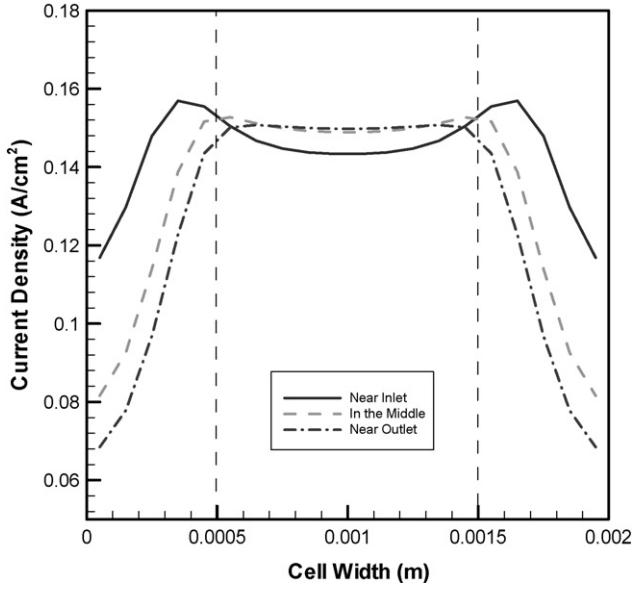

Fig. 6. Current density distribution in the middle of the membrane in both flow and width directions ($\sigma_{backing}$ = 300 S m^{-1}).

become flat because of weak methanol crossover afterwards. Moreover, with lower electronic conductivity, the current density in the membrane shifts to a lower level as well. This performance reduction is caused by the increasing electrical resistance in the backing layer and thus, larger ohmic loss. It is evident that the electronic conductivity shows more important effect on the current density distribution than methanol crossover under the given conditions.

Variations in the current distribution in both flow and width directions are presented in Fig. 6 for the backing layer electronic conductivity of 300 S m^{-1} and cell voltage of 0.4 V. In regions near the inlet and in the middle of the cell, with higher conductivity of the bipolar plate than the backing layer, the highest local current density occurs at the edges between the land and flow channel. On the other hand, near the outlet, due to the severe methanol transport limitation in the land area, the highest current density shift towards the middle of the flow channel.

4. Conclusions

Based on the 3D DMFC model, the electron transport effect in the DMFC is numerically explored, with focus on the impact of in-plane electron transport on the current distribution and cell performance. It was found that the electronic resistance of the backing layer, affected by backing layer electronic conductivity, backing layer thickness and flow channel width, played a relatively important role in determining the current density distribution and cell performance. In order to ignore the electron transport effect on the average current density, the minimum electronic conductivity of the backing layer has to be 1000 S m^{-1}, with the relative error in the average current density less than 5%, under the given conditions. However, such effect will become stronger under higher current density conditions. Future work is needed to examine effects of anisotropic electronic conductivity typically found in fuel cell backing layer materials.

References

[1] J. Wang, R.F. Savinell, in S. Srinivasan, D. D. Macdonald, A.C. Khandkar (Eds.), Electrode Materials and Processes for Energy Conversion and Storage, PV 94-23, 326, The Electrochem. Soc. Proc. Series, Pennington, NJ, 1994.
[2] S.F. Baxter, V.S. Battaglia, R.E. White, J. Electrochem. Soc. 146 (1999) 437.
[3] A.A. Kulikovsky, J. Divisek, A.A. Kornyshev, J. Electrochem. Soc. 147 (2000) 953.
[4] A.A. Kulikovsky, J. Appl. Electrochem. 30 (2000) 1005.
[5] K. Scott, P. Argyropoulos, K. Sundmacher, J. Electroanal. Chem. 477 (1999) 97.
[6] P. Argyropoulos, K. Scott, W.M. Taama, J. Appl. Electrochem. 30 (2000) 899.
[7] J.P. Meyers, J. Newman, J. Electrochem. Soc. 149 (2002) A710.
[8] J.P. Meyers, J. Newman, J. Electrochem. Soc. 149 (2002) A718.
[9] J.P. Meyers, J. Newman, J. Electrochem. Soc. 149 (2002) A729.
[10] W. Liu, C.Y. Wang, J. Electrochem. Soc., in press.
[11] Z.H. Wang, C.Y. Wang, J. Electrochem. Soc. 150 (2003) A508.
[12] C.Y. Wang, P. Cheng, Adv. Heat Transfer 30 (1997) 93.
[13] Z.H. Wang, C.Y. Wang, K.S. Chen, J. Power Sources 94 (2001) 40.
[14] W. Liu, C.Y. Wang, J. Power Sources 164 (2007) 189.
[15] C.Y. Wang, Chem. Rev. 104 (2004) 4727.
[16] H. Meng, C.Y. Wang, J. Electrochem. Soc. 151 (2004) A358.
[17] H. Meng, C.Y. Wang, Fuel Cells 5 (2005) 455.
[18] B.R. Sivertsen, N. Djilali, J. Power Sources 141 (2005) 65.
[19] P.C. Sui, N. Djilali, J. Power Sources 161 (2006) 294.
[20] T. Zhou, H. Liu, J. Power Sources 161 (2006) 444.
[21] H. Meng, J. Power Sources 161 (2006) 466.